Empirical ground-motion prediction equations for Northwestern Turkey using the aftershocks of the 1999 Kocaeli earthquake

D. Bindi [(1)], S. Parolai [(2)], H. Grosser[(2)], C. Milkereit[(2)], E. Durukal [(3)]

[(1)] Istituto Nazionale di Geofisica e Vulcanologia, via Bassini 15, 20133, Milano, Italy

[(2)] GeoForschungsZentrum, Telegrafenberg , D-14473, Potsdam, Germany

[(3)] Boğaziçi University, Kandilli Observatory and Earthquake Research Institute, Department of Earthquake Engineering, 81220, Çengelköy, Istanbul, Turkey

Abstract

We present ground motion models for northwestern Turkey using the aftershocks of the Mw 7.4, 1999 Kocaeli earthquake. We consider 4047 velocity and acceleration records for each component of motion, from 528 earthquakes recorded by stations belonging to regional networks. The ground motion models obtained provide peak ground velocity, peak ground acceleration, and spectral accelerations for 8 different frequencies between 1 and 10 Hz. The analysis of the error distribution shows that the record-to-record component of variance is the largest contribution to the standard deviation of the calibrated ground- motion models. Furthermore, a clear dependence of inter-event error on stress drop is observed. The empirical ground-motion prediction equations, derived for both the larger horizontal and vertical components, are valid in the local magnitude range from 0.5 to 5.9, and for hypocentral distances up to 190 km.

Introduction

Turkey is one of the countries in the Mediterranean region that show the highest level of seismic hazard. In 1999, the northwestern part of the country was struck by two earthquakes, namely the Mw 7.4 Kocaeli and the Mw 7.2 Düzce earthquakes, that caused much damage and many fatalities. Recent studies [e.g *Erdik et al*., 2004; *Parsons*, 2004] showed that the segments of the North Anatolian Fault in the Sea of Marmara to the immediate south of Istanbul have a significant probability (40-65%) of producing a M>7 earthquake within the next 30 years. As a result, several international projects have been promoted for mitigating the seismic risk in this region. The recordings of the Kocaeli and Düzce earthquakes enriched the strong motion data sets exploited for deriving ground-motion models adopted in the hazard calculations performed within these projects. Examples are the empirical ground-motion prediction equations (GrMPEs) recently derived for Europe [Ambraseys et al., 2005], and several domestic models [e.g., Kalkan and Gülkan, 2002, 2004; Özbey et al., 2004]. In this study, 4047 recordings relevant to 528 aftershocks of the Kocaeli earthquake are used to calibrate empirical GrMPEs in the local magnitude range from 0.5 to 5.9 for northwestern Turkey. The empirical GrMPEs are calibrated for peak ground acceleration (PGA), peak ground velocity (PGV) and for the spectral acceleration (SA) of a 5% critical damped oscillator, considering the maximum between the North-South and East-West components, as well as the vertical component. The inter-event and inter-station distributions of error, computed by applying the random-effects approach [Abrahamson and Youngs, 1992] are compared for different choices of the design variables.

Data

The attenuation models are calibrated using 4047 waveforms for each component of motion relevant to 528 earthquakes recorded between August 1999 and December 1999 by 31 stations of the German Task Force for Earthquakes (GTF) and Sabanca-Bolu (SABO) seismic networks, and by 23 accelerometers belonging to the Kandilli Observatory and Earthquake Research Institute (KOERI) strong motion network. The area coverage of the selected data set is shown in Figure 1 (top panel). The GTF and SABO networks consist of 1-Hz geophones (Mark L-4C-3D), a 24-bit digitizer with a sampling rate of 100 sps and Global Positioning System (GPS) timing. The KOERI strong motion network consists of Kinemetrics SSA-12 and GeoSys GSR-16 strong-motion stations working with a sampling rate of 200 sps. The earthquake magnitudes and locations are taken from Bindi et al. [2007] and Parolai et al. [2007]. The distribution of magnitude with distance of the data is shown in Figure 1 (bottom panel). M_L ranges between 0.5 and 5.9 ($1.3 \leq Mw \leq 5.6$), with only 13 earthquakes having $M_L<1.0$, and hypocentral distances up to 190 km are considered. Most of the available data lie in the range 1.5-5 and 10-140 km for magnitude and distance, respectively. The depth of most of the earthquakes is between 5 and 15 km. The waveforms are corrected for the instrumental response and band-pass filtered with a 4th order acausal Butterworth filter between 0.5-25 Hz and 0.1-25 Hz for $M_L \leq 4.5$ and $M_L > 4.5$, respectively.

The stations of the GTF and SABO networks are free-field stations, whereas the KOERI accelerometers are located in the ground floor of small buildings because they were installed mainly for engineering purposes. Most of the stations of the GTF and SABO networks were previously classified as rock or soil [Parolai et al., 2004], whereas NEHRP site classification of the KOERI stations can be found in Durukal [2002]. We extended the existing rock-soil classifications to all stations by analyzing the site responses obtained by applying the generalized inversion technique (GIT) [Parolai et al., 2004, 2007]. Sites were classified as rock (class s_1) if they showed a maximum amplification lower than a certain threshold, otherwise they were classified as soil (class s_2). The geotechnical-geological classification available for some stations was exploited to select the threshold. Since the GIT was carried out while setting to 1 the site response of a single rock-like reference station for the GTF and SABO networks and setting to 1 the average site response for the strong motion network, different thresholds were used for different networks. After some trials, a level of amplification of 2.5 was used for the KOERI network and of 4.5 for the GTF or SABO networks.

Attenuation models

The following ground-motion models are considered [Ambraseys et al., 2005]:

$$\log_{10} Y = a + bM + (c + dM)\log_{10} R_{hypo} + s_{1,2} \pm \sigma_{tot} \qquad (1)$$

$$\log_{10} Y = a + bM + (c + dM)\log_{10}\left(R_{epi}^2 + h^2\right)^{0.5} + s_{1,2} \pm \sigma_{tot} \qquad (2)$$

where *Y* is the variable of interest, that is the PGA, PGV, or SA, M is the magnitude, and R_{epi} and R_{hypo} are the epicentral and hypocentral distances, respectively (in km); σ_{tot} is the standard deviation on $\log_{10}Y$, given by $\sigma_{tot}^2 = \sigma_{eve}^2 + \sigma_{sta}^2 + \sigma_{rec}^2$, where σ^2_{eve}, σ^2_{sta}, and σ^2_{rec} are the inter-event, inter-station and record-to-record components of variance, respectively. The parameter *h* in equation (2) represents a pseudo-depth parameter that accounts for the saturation of Y when R_{epi} becomes small. In equations (1) and (2), the parameters a, b, c, d, h, and the site coefficients $s_{1,2}$, as well as the components of variance, are determined by applying the random effects model [Abrahamson and Youngs, 1992; Chen and Tsai, 2002; Bindi et al., 2006]. The velocity and the acceleration are measured in [m/s] and [m/s^2], respectively. The local magnitude range of the considered data set is 0.5-5.9. Since there is no evidence for earthquakes with M_L <6.0 in Turkey to produce surface ruptures and no systematic studies exist on the determination of the extent of rupture for the events in our data set, in models (1) and (2) we consider the hypocentral and epicentral distances instead of distance to fault. The relationships have been derived for both M_L and Mw, and considering both the maximum between the North-South and East-West horizontal components (H) and the vertical component (V). Finally, since the focal mechanism of the earthquakes used is dominantly strike-slip [Bohnhoff et al., 2006], no factor for the earthquake mechanism is included in the attenuation models (1) and (2), that have to be considered valid for the strike-slip regime.

Results and Discussion

Eight tables including the coefficients obtained for the empirical GrMPEs (1) and (2) are provided as *Electronic Data Supplements*.

Error distributions

Figure 2 exemplifies the analysis of the variances for equation (1) in the case of maximum horizontal SA, considering both M_L and Mw and the epicentral distance. The results show that the total standard deviation σ_{tot} is mainly determined by the record-to-record variability σ_{rec}. The record-to-record variability can be associated to both source effects (e.g. directivity) and propagation effects. Since we analyzed small to moderate size earthquakes recorded at far field distances, we think that the heterogeneities affecting the propagation medium are the main source of the observed ground motion variability for sites that belong to the same class. Figure 2 also shows the behavior of the standard deviation of the inter-event distribution of error (σ_{eve}) with frequency. The inter-event distribution of error, which weakly contributes to the total error, assumes a specific value for each earthquake and it is due to the correlation between the errors for different recordings of the same earthquake. Then, the value of σ_{eve} reflects the variability of the ground motion between earthquakes having the same magnitude, and the analysis of σ_{eve} as a function of frequency can provide some information about the variability of the source characteristics. For $f < 1$ Hz, σ_{eve} increases with decreasing frequencies for both Mw and M_L. For 1 Hz $\leq f \leq$ 5 Hz, σ_{eve} is almost constant and similar for both the Mw and M_L regressions. For frequencies > 5Hz, σ_{eve} increases when the regression is performed considering Mw, while it starts to increase only after 10 Hz when M_L is used. The dependence of σ_{eve} with frequency can be explained by considering both the frequency range spanned by the corner frequency f_c of the considered earthquakes [Figure 4 in Parolai et al., 2007] and the characteristic frequency band used for the computation of M_L and Mw. In fact, considering the response of the Wood-Anderson seismometer (which acts as a high pass filter for displacement with a corner frequency *fc* at 1.25 Hz) and the range of frequency in which most of the *fc* are lying (1Hz$<fc<$10 Hz), M_L estimates reflect mainly source properties for frequencies between 1 and 10 Hz. The increase of σ_{eve} when Mw is used for the regression, starts at lower frequencies because Mw is estimated from the low frequency spectral level. It follows that earthquakes having the same Mw can show differences in the spectral amplitudes at higher frequencies due to stress-drop variations. Causes for the increase of σ_{eve} below 1 Hz are the low signal-to-noise ratio of the acceleration spectra, the effect of the Wood-Anderson high-pass filter, and the uncertainties affecting Mw for the largest earthquakes of the data set, due to the too-narrow low-frequency plateau that is exploitable for the seismic moment estimation.

Another result from Figure 2 is that σ_{rec} for the Mw and M_L regressions are similar. This was expected since σ_{rec} is not related to the source properties of a specific earthquake. Considering that Figure 2 show that σ_{rec} provides the main contribution to σ_{tot} , it follows that σ_{sta} has a negligible contribution, similar to σ_{eve} (see the Electronic Supplements).

Stress drop dependence of σ_{eve}

In order to investigate the influence of the stress drop on σ_{eve}, the inter-event error distribution for the regression carried out on PGA, while considering the maximum horizontal component, the epicentral distance and both M_L and Mw, is shown in Figure 3. The source parameters $\Delta\sigma$ and Mo are taken from Parolai et al. [2007]. We emphasise the results obtained for PGA since this is the parameter that is most affected by stress-drop variations. The errors, defined such that their absolute value must be greater than 10% of the maximum absolute error, so as to make the graphical presentation clearer, are shown in Figure 3 against M_L and the stress drop $\Delta\sigma$ of the circular Brune [1970] model for the M_L regression, and against the seismic moment Mo and $\Delta\sigma$ for the Mw regression. Figure 3 shows that, for a given M_L or Mw, the inter-event errors show the tendency to range from negative (over-estimation) to positive (under-estimation) values, depending on $\Delta\sigma$. Low stress drops are associated to negative errors while positive errors are observed for high stress drops. The range spanned by $\Delta\sigma$ depends on magnitude and generally increases with increasing magnitude.

Site classification dependence of σ_{sta}

The inter-station distribution is evaluated twice; first without considering the site classification, and second after introducing the two site classes. The site classification allows for a significant reduction of the errors, and the standard deviation of the error distribution of GTF and SABO stations is reduced from 0.21 to 0.14. The inter-station errors for the KOERI network are smaller than 0.1 and are less affected by the classification. The coefficients for the calibrated SA models are provided in the Supplement for 8 frequencies between 1 and 10 Hz.

Empirical GrMPEs

Figure 4 compares the predicted PGA for a rock site resulting from a Mw=5.2 earthquake with the predictions from the Özbey et al [2004] (hereinafter Özb04) and Ambraseys et al. [2005] (hereinafter Amb05) relationships. We selected Mw=5.2 because it is larger than the minimum magnitude for Özb04 and Amb05 (Mw>5), but the corresponding M_L (about 5.5) is still within the range of validity of our model. Özb04 was derived by considering the Kocaeli and Düzce earthquakes and their strongest aftershocks (17 earthquakes in all), whereas Amb05 was derived considering earthquakes that occurred in Europe and Middle East. Both relationships are derived for Mw>5 and for the closest distances from the fault. Since for a magnitude 5.2 the correction for the difference between the epicentral distance and the closest distance from the fault is expected to be negligible [Scherbaum et al., 2004], we do not apply any statistical corrections for the difference between the metrics. A comparison with empirical GrMPEs derived for other regions is beyond the aim of the present article. Anyway, a comparison between regional empirical GrMPEs derived for similar tectonic regime in Western United States (e.g. Sadigh et al. [1997]) can be found in Özb04. More recent comparisons can be found in the reports of the Next Generation Attenuation (NGA) models project developed by the Pacific Earthquake Engineering Research Center (PEER), available at http://peer.berkeley.edu. Figure 4 shows that, for an earthquake of Mw=5.2, the Amb05 relationship is in good agreement with the local relationship calibrated in the present study, whereas the Özb04 relationship under-estimates the PGA, especially at distances <20 km. Indeed, in the Kocaeli earthquake the recorded near field ground motion levels were lower than the ones predicted by empirical GrMPEs, while the recorded level were in agreement with the empirical GrMPEs for larger distances [Durukal, 2002]. Since Özb04 relationship uses records from M>5 events from the Kocaeli sequence, the discrepancy between our model and Özb04 model was expected. The agreement between Amb05 and Özb04 improves with increasing Mw, and they are almost coincident for Mw=7.4. An attempt to extrapolate the relationship calibrated in this study to events of Mw=7.4 resulted in PGA values being overestimated with respect to the Amb05 and Özb04, suggesting that extrapolating empirical GrMPEs to well outside their calibration magnitude range is not viable.

Conclusions

New ground-motion prediction equations have been calibrated using a large data set of aftershocks following the 1999 Kocaeli earthquake. To avoid the use of corrective factors for the metrics and the earthquake size when parametric seismic catalogs are used for hazard assessment studies, the models have been calibrated considering both the local and moment magnitudes, as well as the epicentral and hypocentral distances. The equations can be applied to Northwestern Turkey for events within the local magnitude range 0.5-5.9 and for hypocentral distances up to 190 km. Although the magnitude range spanned in this study may appear to limit the applicability of the obtained empirical GrMPEs, we recall that recent moderate earthquakes have occurred in different regions of the world (e.g., the September 7, 1999 Ms=5.9 Athens earthquake; the 26 May, 2006 M_L =6.2 Indonesia earthquake), causing severe damage and loss of life and hence have shown the importance of reliable local ground-motion prediction equations for the earthquake hazard assessment. The earthquake hazard in Northern Marmara is dominated by the North Anatolian Fault. The probability of occurrence of a $M>7$ earthquake within the next 30 years is estimated as (40-65%) [Parsons, 2004]. This certainly does not exclude the possibility that moderate size earthquakes take place near Istanbul and elsewhere in Northwestern Turkey. In terms of the study area covered in this work, a moderate earthquake occurring in the vicinity of Istanbul may lead to considerable building damage, casualties and losses. The development of adequate empirical GrMPEs for small to moderate size earthquakes is also important for Monte-Carlo-type simulations involving ground motion predictions for a family of earthquake events representative of regional earthquake statistics for a wide magnitude range. Such considerations are particularly used in loss estimations carried out for insurance purposes. Although it may be argued that the direct applicability of an empirical GrMPEs estimated from aftershocks to independent events is questionable, this is certainly a research area that needs further attention.

The analysis of the error distribution showed that the record-to-record component of variance is the largest contribution to the variance of the calibrated ground- motion models. Moreover, although the contribution of the inter-event component of error to the total error is negligible, it is correlated to the stress-drop variability and it is higher when the regressions are performed considering the moment magnitude than when local magnitude is used.

Acknowledgments

This work was partially funded by the project CEDIM: Megacity Istanbul (http://www.cedim.de) and by the Hannover Re, the German Research Foundation, and the General Directorate of Disaster of Turkey. We thank D. Boore and an anonymous reviewer for their useful suggestions. K. Fleming kindly improved our English.

References

Abrahamson N. A., Youngs R. R. (1992). A stable algorithm for regression analyses using the random effects model. *Bull Seism. Soc. Am.* 82, 505-510.

Ambraseys, N. N., J. Douglas, S. K. Sarma and P. M. Smit (2005). Equations for estimation of strong ground motions from shallow crustal earthquakes using data from Europe and Middle East: horizontal peak ground acceleration and spectral acceleration, *Bull. of Earth. Engineering*, 3, 1-53.

Bindi, D., S. Parolai, E. Görgün, H. Grosser, C. Milkereit, M. Bohnhoff, and E. Durukal (2007). M_L scale in Northwestern Turkey from 1999 Izmit aftershocks: updates, *Bull. Seism. Soc. Am.*, in press.

Bindi, D., L. Luzi, F. Pacor, G. Franceschina and R. R. Castro (2006). Ground motion predictions from empirical attenuation relationships versus recorded data: the case of the 1997-98 Umbria-Marche (Central Italy) strong motion data-set. *Bull Seism. Soc. Am.* 96, 984-1002, doi: 10.1785/0120050102

Bohnhoff M., H. Grosser and G. Dresen (2006). Strain partitioning and stress rotation at the North Anatolian fault zone from aftershock focal mechanisms of the 1999 Izmit Mw=7.4 earthquake, *Geophys. J. Int.* 166, 373-385.

Brune, J. N. (1970), Tectonic stress and the spectra of seismic shear waves from earthquakes, *J. Geophys. Res*., 75, 4997-5009.

Chen, Y-H., and C-C. P. Tsai (2002), A new method for estimation of the attenuation relationship with variance components, *Bull Seism. Soc. Am.* 92, 1984-1991.

Durukal E. (2002). Critical evaluation of strong motion in Kocaeli and Duzce (Turkey) earthquakes. *Soil Dynamics and Earthquake Engineering* 22 (7): 589-609.

Erdik, M., M. Demircioglu, K. Sesetyan, E. Durukal, B. Siyahi (2004), Earthquake hazard in Marmara region, Turkey, *Soil. Dynam. Earthquake Eng*., 24, 605-631.

Kalkan E., and P. Gülkan, 2002. Attenuation modeling of recent earthquakes in Turkey, *J. of Seism.* 6, 397-409

Kalkan, E., and P. Gülkan (2004). Empirical attenuation equations for vertical ground motion in Turkey, *Earthquake Spectra* 20, 853-882.

Özbey, C., A. Sari, L. Manuel, M. Erdik, and Y. Fahjan (2004). An empirical attenuation relationship for Northwestern Turkey ground motion using a random effects approach, *Soil. Dynam. Earthquake Eng*. 24, 115-125.

Parolai, S., D. Bindi., M. Baumbach, H. Grosser., C. Milkereit, S. Karakisa, S. Zünbül (2004). Comparison of different site response techniques using aftershoks of the 1999 Izmit earthquake, *Bull. Seism. Soc. Am*. 94, 1096-1108.

Parolai S., D. Bindi, E. Durukal, H. Grosser, and C. Milkereit (2007). Source parameters and seismic moment-magnitude scaling for Northwestern Turkey, *Bull. Seism. Soc. Am*. in press

Parsons, T. (2004), Recalculated probability of M≥7 earthquakes beneath the Sea of Marmara, Turkey, *J. Geophys. Res.* 109, B05304, doi:10.1029/2003JB002667.

Sadigh K., C-Y Chang, J.A. Egan, F. Makdisi, and R. R. Youngs (1997). Attenuation relationships for shallow crustal earthquakes based on California strong motion data, *Seism Res Le*tt 68, 180-189.

Scherbaum, F., J. Schmedes, F. Cotton (2004). On the conversion of source-to-site measures for extended earthquake source models, *Bull. Seism. Soc. Am. 94*, 1053-1069.

Figure captions

Figure 1. Top: Epicenter location (black dots), GTF and SABO seismological (triangles) and KOERI strong motion (squares) stations. Bottom: local magnitude versus hypocentral distance distribution.

Figure 2. Standard deviation σ_{tot} for the maximum horizontal SA (epicentral distance, equation 2), considering M_L (gray line) and Mw (black line). The standard deviation σ_{eve} (circle) of the inter-event distribution and the standard deviation σ_{rec} (square) of the record-to-record distribution of error are shown for M_L (gray) and Mw (black).

Figure 3. Inter-event errors for the maximum horizontal PGA model, considering epicentral distance. The amount of error is given by the color of the symbol. Top: Mw is considered in the regression. The errors having absolute values >0.04 are shown as a function of the stress drop $\Delta\sigma$ and the seismic moment Mo of each earthquake. Bottom: M_L is considered in the regression. The errors having absolute values >0.02 are shown as a function of $\Delta\sigma$ and M_L. The source parameters are taken from Parolai et al. [2007].

Figure 4. Comparison between the mean PGA ± one standard deviation predicted by Ambraseys et al. [2005], Özbey et al [2004] and this study for a Mw=5.2 earthquake.

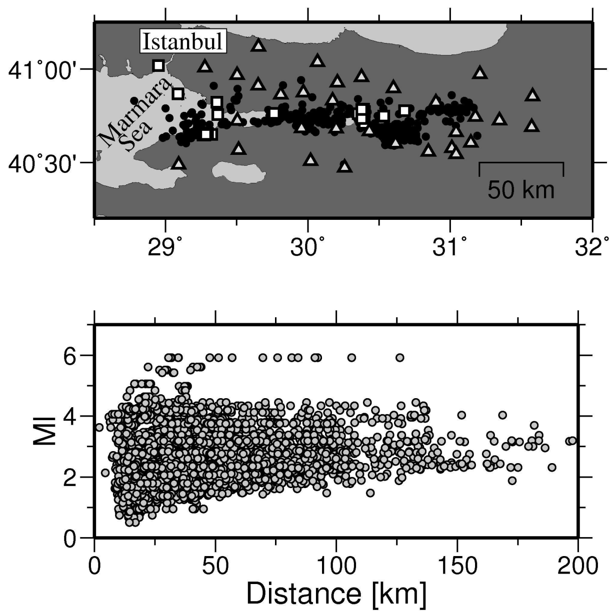

Istanbul
Marmara Sea
41˚00'
40˚30'
50 km
29˚
30˚
31˚
32˚
Ml
0
2
4
6
0
50
100
150
200
Distance [km]

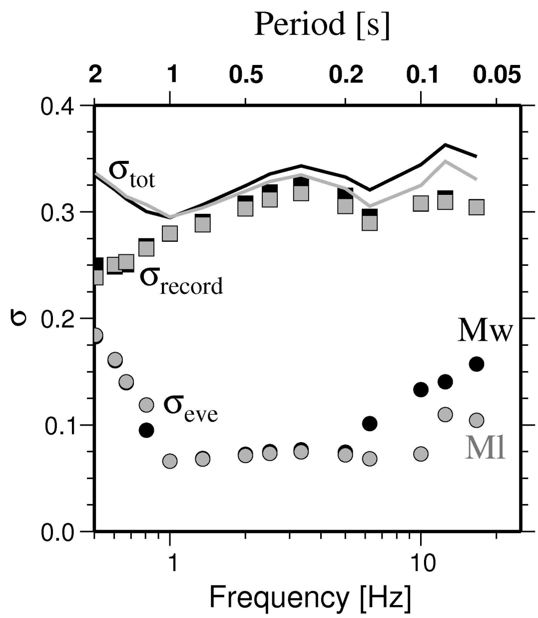

Period [s]
2
1
0.5
0.2
0.1
0.05
0.4
0.3
0.2
0.1
0.0
σ
σ_{tot}
σ_{record}
σ_{eve}
Mw
Ml
1
10
Frequency [Hz]

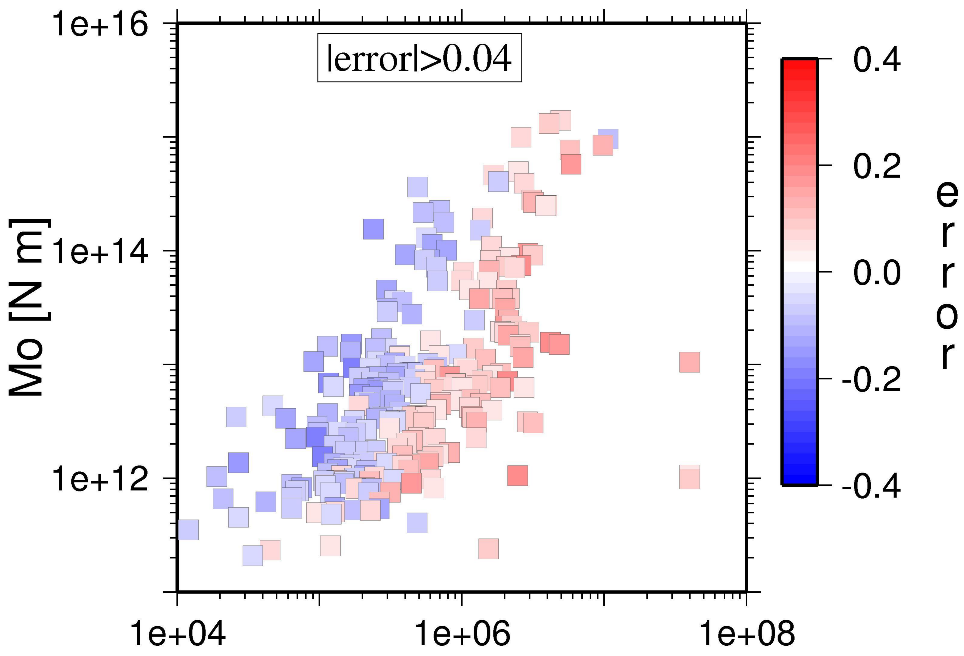

|error|>0.04
1e+16
1e+14
1e+12
Mo [N m]
1e+04
1e+06
1e+08
0.4
0.2
0.0
-0.2
-0.4
error

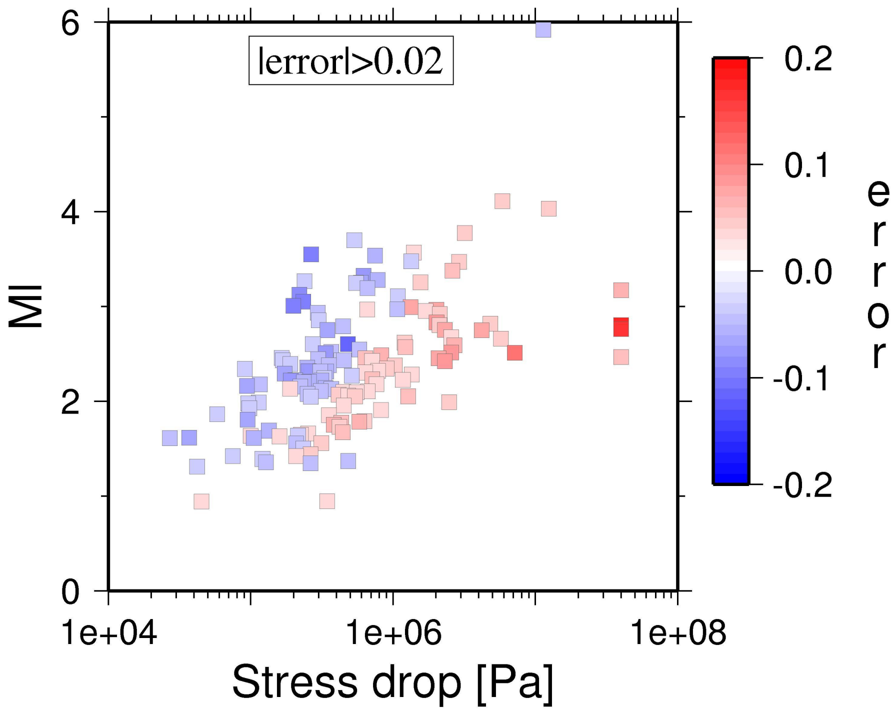

|error|>0.02
6
4
2
0
Ml
1e+04
1e+06
1e+08
Stress drop [Pa]
0.2
0.1
0.0
-0.1
-0.2
error

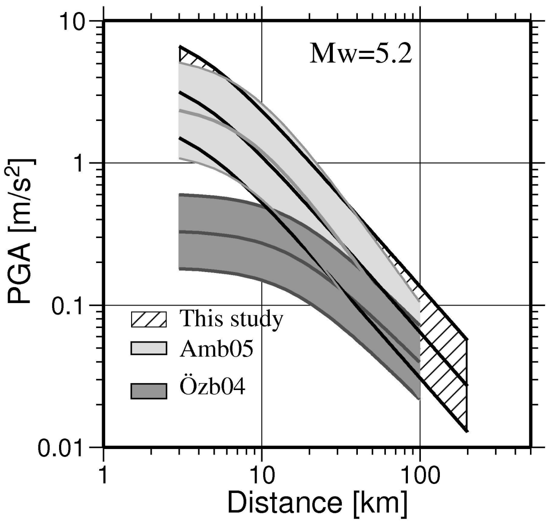

Mw=5.2
PGA [m/s^2]
10
1
0.1
0.01
1
10
100
Distance [km]
This study
Amb05
Özb04